Egypt. J. Chem. **Vol. 65,** No. 2 pp. 389 - 398 (2022)

Egyptian Journal of Chemistry

http://ejchem.journals.ekb.eg/

Synergistic Effect of Chitosan Biguanidine Hydrochloride Salt as a Green Inhibitor for Stainless Steel Alloy Corrosion in a 0.5 M H_2SO_4 Solution

Ahmed El Nemr[1,*], Abdualah Elhebshi[2], Mohamed S. El-Deab[3], Ibrahim Ashour[2], Safaa Ragab[1]

1 Environmental Division, National Institute of Oceanography and Fisheries (NIOF), Kayet Bey, El-Anfoushy, Alexandria, Egypt, ahmed.m.elnemr@gmail.com

2 Chemical Engineering Department, Faculty of Engineering, Elminia University, Elminia, Egypt,

3 Department of Chemistry, Faculty of Science, Cairo University, Cairo, Egypt

Abstract

The inhibition efficiency (IE) of the hydrochloride salt of chitosan biguanidine (CBG-HCl, a green organic compound) on stainless steel alloy (SS) corrosion in 0.5 M H_2SO_4 solution was documented in this work. Data reported for electrochemical impedance spectroscopy (EIS) and potentiodynamic analysis confirmed increasing of the corrosion resistance of stainless steel in 0.5 M H_2SO_4 solution in the presence of CBG-HCl with a synergistic effect of KI. Potentiodynamic experiments also indicate that the blend of CBG-HCl-KI works as a mixed-type inhibitor for stainless steel alloy corrosion. The best information gathered agreed with the Langmuir isotherm model. The corresponding normal Gibbs inhibitor adsorption free energy implied that the processes are random and involved two forms of interactions, chemisorption and physisorption. The highest inhibition efficiency (88 %) in this work was reported for 400 ppm of CBG-HCl blended with 800 ppm KI. In fact, with a long immersion time, the efficiency of CBG-HCl inhibition remains effectively high, demonstrating its good stability in the 0.5 M H_2SO_4 medium.

Keyword: Chitosan biguanidine; Stainless steel; Corrosion inhibitor; Synergistic effect; EIS; Potentiodynamic

1. Introduction

Stainless steel (SS) has been used in wide applications in industries and machinery. It has high resistance to corrosion due to the protective oxide film formed by the chromium element exists in SS alloy. Pitting corrosion is the serious failure of SS, which occurs as a result of the breakdown of the oxide film in aggressive acidic media [1,2].

The use of corrosion inhibitors in oil and industrial processes (such as pickling operations, acid washing, acidification of oil and gas wells to remove rust and scales) is a famous way to regulate the corrosion rate in acidic solutions [3-5]. Corrosion inhibitor defense also relies on the alteration of metallic surfaces to form a protective layer by the sorption process of the inhibitor molecules. Quantitative structure–activity relationship (QSAR) was used to study the mechanism of defence and in the inhibition efficiency prediction of some organic compounds [6-13]. Some of the inhibitors of applied natural product corrosion include hetero atoms such as atoms of sulfur, nitrogen, oxygen and phosphorus that increase the absorption of inhibitor compounds on the metal surfaces [14-17]. As environmentally friendly corrosion protection, several organic compounds and plant extracts are used as corrosion inhibitors [18-25]. Chitin and its derivatives derived chitosan are commonly used in the medicine, cosmetics, textiles, and food industries [26]. Due to its greater number of adsorption sites and ecological friendliness, chitosan and its derivatives have been studied as a corrosion inhibitor [17, 27-28]. However, chitosan is poorly soluble in water which may limit its use as an inhibitor of metals corrosion, thus we can use derivatives of chitosan that mainly have good solubility in water may solve the problem of dissolving chitosan in the water while maintaining the number of adsorption sites in chitosan which can increase the efficiency of chitosan as a corrosion inhibitor [29–33].

Research has focused on the production of affordable, stable, and minimally negative environmental impacts of green corrosion inhibitor compounds due to global concern about health derivatives) [17, 34-42] as a green inhibitor in acidic

*Corresponding author (A. El Nemr) e-mail: ahmedmoustafaelnemr@yahoo.com; ahmed.m.elnemr@gmail.com
Receive Date: 24 July 2021, Revise Date: 21 August 2021, Accept Date: 23 August 2021
DOI: 10.21608/EJCHEM.2021.87235.4219

media for stainless steel alloys corrosion and for assessing the effectiveness and mechanism of CBG-HCl as an inhibitor of corrosion. The novelty of our work is from the investigation of the generalization of the use of CBG-HCl as a green corrosion inhibitor, which we employed in a previous study of carbon steel corrosion resistance in an acidic environment and found to be very effective. As a result, we are eager to demonstrate its use as a green corrosion inhibitor for stainless steel in order to expand its application in industries.

2. Experimental

2.1. Solutions and Chemicals

Polymer CBG-HCl (Fig. 1), 100% pure crystals, was used as an eco-friendly corrosion inhibitor. The inhibitor was prepared in the lab and its crystals were grounded to powder then the inhibitor solution was obtained by dissolving the specific amount of CBG-HCl powder in 0.5 M H_2SO_4 [17]. The corrosive solution (electrolyte) 0.5 M H_2SO_4, was obtained by diluting commercial sulfuric acid (98%) using deionized water.

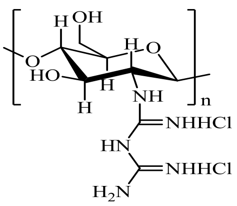

Fig. 1. CBG-HCl chemical structure.

2.2. Electrochemistry, alloy, corrosion cell, and machine tools

A stainless-steel alloy (SS) rod – with the element composition (wt %): 71.08 Fe, 18.245 Cr, 0.005 S, 1.17 Mo, 0.11 Cu, 8.25 Ni, 0.85 Mn, 0.06 Ti, 0.02 Al, 0.06 V, 0.17 C – has been applied as the working electrode. Stainless steel alloy working electrode was covered by a Teflon layer, leaving 0.8 cm^2 of two-dimensional exposed surface area. A graphite electrode (1 cm diameter × 15 cm length tall) and a saturated calomel electrode (SCE) were, respectively, used as counter and reference electrodes.

A glass corrosion cell of three-electrode connected to Gamry Potentiostat/Galvanostat (model Series-G 300) controlled by Gamry Fram work version 6.12 software was applied to investigate the electrochemical measurements of the inhibitor activity. For impedance measurements using an open circuit potential (OCP) condition of stainless-steel alloy (SS) working electrode, the frequency ranged from 0.1 Hz to 100 kHz with a peak-to-peak amplitude of 10 mV using AC signals. The equivalent circuit software was used to analyse the impedance spectra of the CBG-HCl corrosion inhibition and the KI synergistic effect.

2.3. Methodology of experiments

The working electrode was prepared from stainless steel alloy (SS) and cleaned before the test using wet SiC papers of progressively finer grades before each test, rinsed with deionized water, thoroughly rinsed with ethanol in an ultrasonic bath and then dried and submerged in the 0.5 M H_2SO_4 solution. The media contained 0.5 M H_2SO_4 with various concentrations of CBG-HCl (100, 200, 400 and 600 ppm) dissolved in distilled water was prepared. All of the data recorded in the present study (impedance, current, resistance) are related to the working electrode surface area geometry. At room temperature (25 °C) the electrochemical tests were carried out. After achieving a steady value performed by submerging the working electrode in the test media of around 30 minutes, the free corrosion potential, EIS and polarization measurements were measured. Potentiodynamic polarization curves were studies using a scan rate of 5 mV/s starting from the OCP to the cathodic direction (approximately –250 mV vs. OCP), followed by the reversed potential scan to a final potential of approximately +250 mV against OCP.

3. Results and discussion

3.1. Electrochemical Impedance Spectroscopy (EIS) studies

The IE percentage of corrosion using CBG-HCl as an inhibitor for the stainless-steel electrode surface in 0.5 M H_2SO_4 media, EIS experiments were carried out in this study. At OCP, EIS assays were made out in a broad frequency ranged between 0.10 Hz and 100 kHz, with an amplitude of AC voltage of ±10 mV. Before conducting the test at room temperature, the stainless-steel electrode was optimized at OCP for 30 minutes. EIS data shown in Fig. 2 as a Nyquist diagram, recorded on a stainless-steel working electrode in the acidic media in the absence and presence of100, 200, 400 and 600 ppm of CBG-HCl, while Fig. 3 presents the results under the same conditions with a synergistic effect of 800 ppm of KI. The figures indicate that the semicircle diameter increases with a rise in the concentration of the CBG-HCl in the electrolyte, suggesting that the CBG-HCl forms a protective adsorption film and that the corrosion resistance of the metal increases.

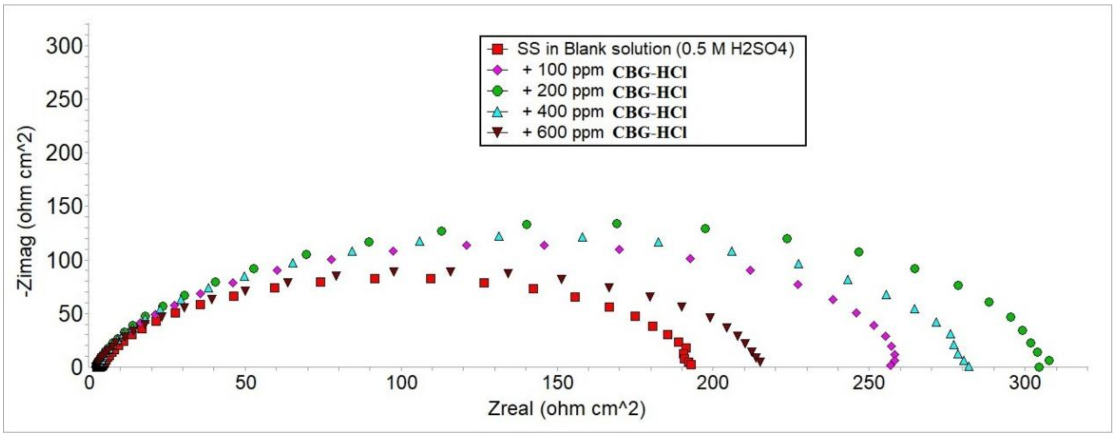

Fig. 2.Nyquist SS plot reported for various CBG-HCl concentrations in 0.5 M H_2SO_4 at 298 K.

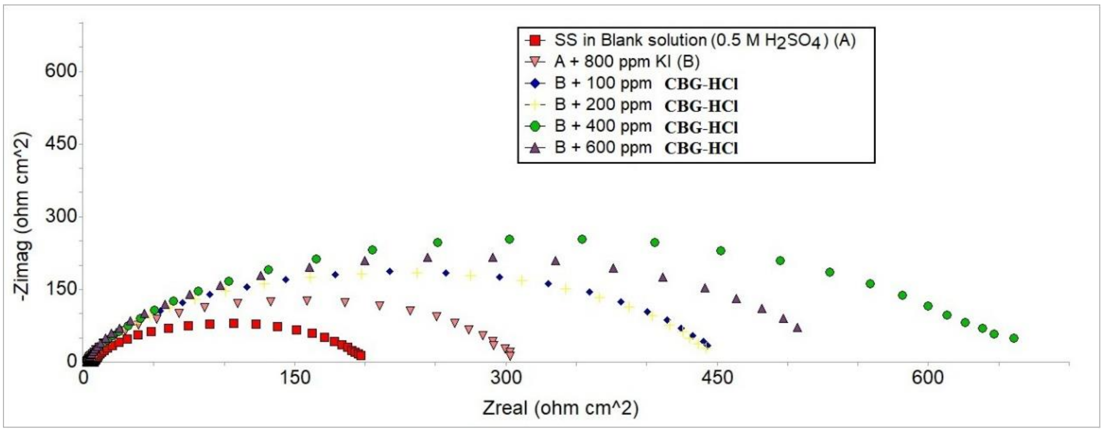

Fig. 3. Nyquist SS plot reported for the synergistic effect of 800 ppm of KI at different CBG-HCl concentrations in 0.5 M H_2SO_4 at 298 K.

The electrical equivalent circuit (EEC) as seen in Fig. 4 was applied for the EIS data simulation and to determine the equivalent resistance and, using equation (1) [43], the corresponding efficiencies were measured and reported in Tables 1 and 2. R_{el} is the ohmic resistance in the EEC between the SCE and the stainless steel working electrode; R_1 is the resistance of the corrosion reaction-related charge transfer at OCP; CPE1 is the electrode/electrolyte interface electrical double-layer capacitance [44].

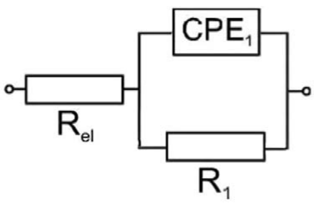

Fig. 4. EEC model was applied to represent EIS information collected on stainless steel electrodes immersed in 0-containing electrolytes and different inhibitor concentrations. Where, respectively, R_{el}, R_1 and CPE1 reflect solution resistance, polarization resistance, and double-layer capacitance.

$$IE\% = (1- [\frac{R_1^{(b)}}{R_1^{(in)}}]) \times 100 \qquad (1)$$

Where $R_1^{(b)}$ and $R_1^{(in)}$ are respectively, the polarization resistances in the absence and the presence of the CBG-HCl.

Table 1. The equivalent circuit and determined IE parameters of stainless-steel working electrode in 0.5 M H_2SO_4 with different concentrations of CBG-HCl as inhibitor.

Electrolyte composition	R_1 ($\Omega\ cm^2$)	CPE×10^6($\Omega^{-1}cm^{-2}S^{\alpha}$)	α	IE %
Blank (0.5M H_2SO_4)(A)	191	426	0.893	-
A+ 100 ppm CBG-HCl	264	354	0.899	27.65
A+ 200 ppm CBG-HCl	310	303	0.902	38.39
A+ 400 ppm CBG-HCl	283	323	0.901	32.51
A+ 600 ppm CBG-HCl	215	248	0.888	11.16

Table 2. The equivalent circuit and determined IE parameters of stainless-steel working electrode in 0.5 M H_2SO_4 with different concentrations of CBG-HCl as inhibitor in the presence of 800 ppm KI.

Electrolyte composition	R_1 ($\Omega\ cm^2$)	CPE×10^6($\Omega^{-1}cm^{-2}S^{\alpha}$)	α	IE %
Blank (0.5M H_2SO_4)	191	426	0.893	0.00
Blank + 800 ppm KI (B)	306	420	0.883	37.58
B + 100 ppm CBG-HCl	452	382	0.867	57.74
B + 200 ppm CBG-HCl	448	351	0.873	57.37
B + 400 ppm CBG-HCl	647	190	0.856	70.48
B + 600 ppm CBG-HCl	526	333	0.886	63.69

3.2. Potentiodynamic measurements

To check the data obtained from EIS measurements, potentiodynamic experiments have been performed. Fig. 5 shows potentiodynamic curves observed in a 0.5 M H_2SO_4 solution on a stainless-steel working electrode at different amounts of CBG-HCl in the electrolyte. From the bends in Fig. 5, it is clear that with the rise of the CBG-HCl concentration in the solution, only the anodic current decreases. The other side of Fig. 6 shows the effects of the curves with a synergistic effect of 800 ppm of KI for the same conditions. Just in Fig. 6 as the inhibitor concentration rises, the current decreases for both the anodic and cathodic reactions, which proves that the blend of CBG-HCl-KI was worked as a corrosion inhibitor of the mixed-type process. The corresponding densities of the corrosion current (j) were predicted by extrapolating the anodic and cathodic curves to the related OCP and the data are presented in Table 3 with the calculated IE% obtained from Eq. (2) [17, 43, 45].

$$IE\% = (1 - \frac{j_{in}}{j_b}) \times 100 \qquad (2)$$

Where j_{in} (A cm^{-2}) is the current of corrosion of a specific CBG-HCl concentration and j_b is the current of corrosion in absence of CBG-HCl (blank solution).

3.3. Adsorption isotherm

Temkin, Langmuir, and Freundlich isotherm models were conducted to identify the CBG-HCl inhibitor adsorption on the surface of a stainless-steel working electrode. The adsorption isotherm of Langmuir best agreed with the results, which assume that the IE% is directly proportional to the surface coverage θ by the inhibitor [46, 47]. The linear form of the Langmuir isotherm model is presented by Eq. (3) [48] and the plot between C/θ and C is presented in Fig. 7.

$$\frac{C}{\theta} = \frac{1}{K_{ads}} + C \qquad (3)$$

Where C, θ, and K_{ads} are respectively, the CBG-HCl concentration, the surface coverage, and the constant of adsorption equilibrium. The inhibitor is considered to follow Langmuir if the plot between C/θ and C is linear and the slope of the line and the correlation coefficient (R^2) are closed to unity. Similarly, for Temkin the plot between θ and log C and for Freundlich the plot between log θ and log C should be linear if they were applicable to the adsorption data of an inhibitor to a metal surface. The Langmuir isotherm is best fitted into the experiment data with R^2 of 0.9884 and slope 1.2698 derived from plots in Fig. 7 and the isotherm data is shown in Table 4. This proved a monolayer inhibitor adsorption on the stainless-steel surface.

Equilibrium constant of adsorption K_{ads}= 0.4831 dm^3mg^{-1} ($L mg^{-1}$) produced from the intercept of the line in Fig. 7, and standard Gibbs free energy (ΔG^0_{ads}) of adsorption (kJ mol^{-1}) was obtained from Eq. (4) [49].

$$K_{ads} = \frac{1}{C_{solvent}} \exp\left(\frac{-\Delta G^0_{ads}}{RT}\right) \quad (4)$$

Where T, $C_{solvent}$, and R (J $mol^{-1}K^{-1}$) are respectively, the temperature (K), the molar concentration of the solvent, which in this case, is water (C_{H2O}= 10^6 $mgdm^{-3}$), and R the gas constant. On the low carbon steel surface, the estimated standard Gibbs free adsorption energy of the inhibitor was –32 kJ mol^{-1}) at 298 K. Published data showed that charging sharing between the molecules and the metal (chemisorption) involves magnitudes of normal Gibbs free adsorption energy in an aqueous medium around or higher (more negative) than –40 kJ mol^{-1} while around –20 kJ mol^{-1} or lower indicate electrostatic interaction adsorption between the inhibitor and metal [50, 51]. Consequently, the related determined value of standard Gibbs free adsorption energy (–32 kJ mol^{-1}) indicates that CBG-HCl adsorption requires two forms of interactions, chemisorption and physisorption, and the negative values of ΔG^0_{ads} guarantee the mechanism of the adsorption spontaneity and the durability of the inhibitor monolayer adsorbed on the stainless-steel electrode surface [48].

Table 3. Corrosion current density (j) obtained from potentiodynamic measurements recorded on SS surface in a 0.5 M H_2SO_4 solution of different amounts of CBG-HCl and in presence of synergistic effect of 800 ppm of KI with Linked performance values for corrosion inhibition.

Electrolyte composition	Corrosion current density (j) (mA cm^{-2})	Inhibition Efficiency (%)
Blank (0.5M H_2SO_4)(A)	0.090	-
A + 100 ppm CBG-HCl	0.059	34.44
A + 200 ppm CBG-HCl	0.052	42.22
A + 400 ppm CBG-HCl	0.057	36.67
A + 600 ppm CBG-HCl	0.075	16.67
A + 800 ppm KI (B)	0.044	51.11
B + 100 ppm CGB-HCl	0.034	62.22
B + 200 ppm CBG-HCl	0.033	63.33
B + 400 ppm CBG-HCl	0.023	74.44
B + 600 ppm CBG-HCl	0.038	57.78

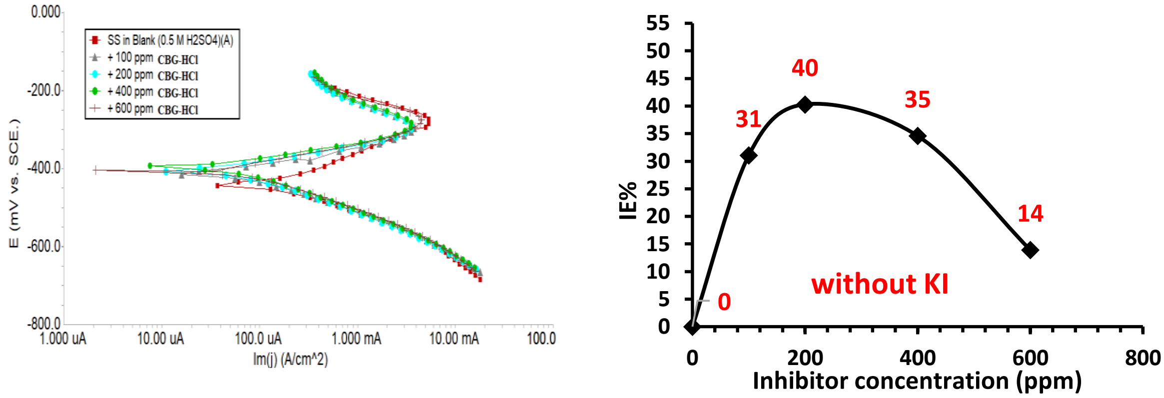

(a) (b)

Fig. 5. (a) Stainless steel electrode potentiodynamic plots were reported at different CBG-HCl concentrations in a 0.5 M H_2SO_4 solution. Rate of scan = 5 mV/s, (b) The average IE% values of CBG-HCl on SS in 0.5 M H_2SO_4 solution. The data represent the average IE% values obtained using EIS and potentiodynamic experiments conducted at 100, 200, 400 and 600 ppm concentration of CBG-HCl.

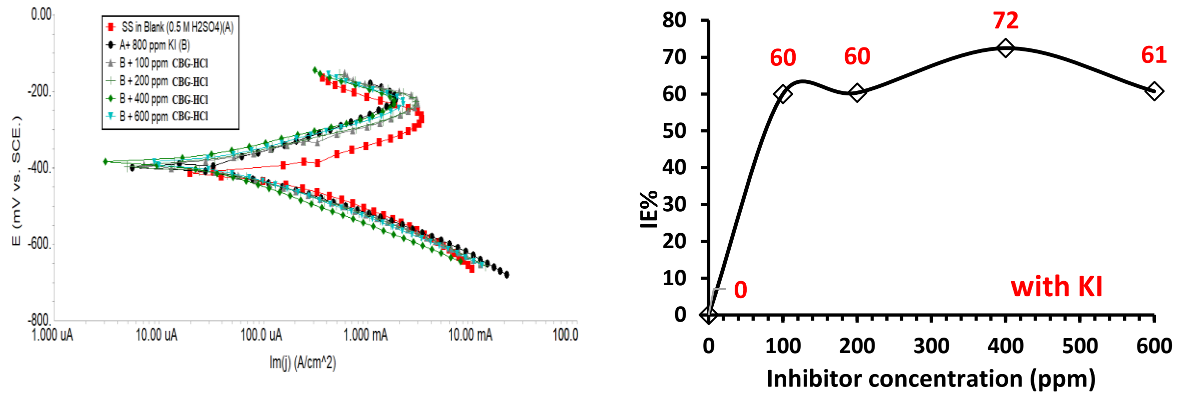

(a) (b)

Fig. 6. (a) Potentiodynamic SS electrode plots were performed at different CBG-HCl concentrations together with 800 ppm KI in 0.5 M H_2SO_4 solution. Rate of scan = 5 mV/s. (b) The average IE% obtained using EIS and potentiodynamic experiments conducted at 100, 200, 400 and 600 ppm of CBG-HCl concentration and together with 800 ppm KI on SS in 0.5 M H_2SO_4 solution.

Table 4. Adsorption isotherms parameters at 298K.

Langmuir		Temkin		Freundlich	
R^2	Slope	R^2	Slope	R^2	Slope
0.9884	1.2698	0.75	0.1993	0.75	0.1315

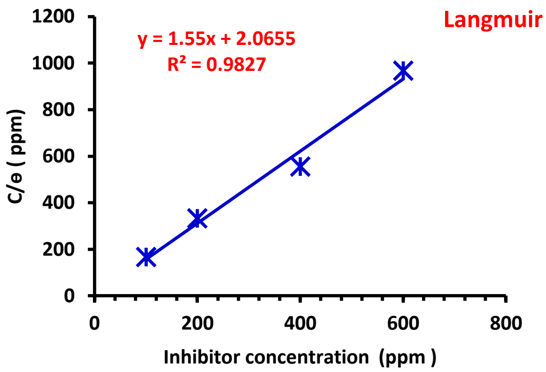

Fig. 7. Langmuir isothermal model plot for CBG-HCl inhibitor on the surface of stainless-steel alloy in acidic media.

3.4. Stability of inhibition efficiency

In the case of 400 ppm CBG-HCl concentration in a 0.5 M H_2SO_4 solution, electrochemical impedes spectroscopy (EIS) experiments were performed at different contact times to investigate the time necessary for the CBG-HCl to achieve optimum inhibition efficiency and durability under test conditions. Table 5 and Fig. 8 present the associated IE% and corrosion resistance (R_p, ohm cm^2) values. The data shows that the corrosion inhibition efficiency (IE%) reached 82.3 % after 30 minutes of contact time between the stainless-steel working electrode and the corrosive environment. The highest efficiency was reported after four hours of immersing time (about 88.3%), and remained stable after 72 hours, which is the recommended immersion time in the acid cleaning for removal of scale in the desalination industry.

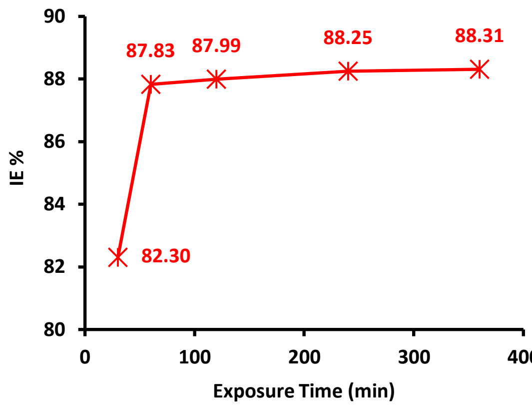

Fig. 8. EIS inhibition performance of a stainless-steel electrode immersed in a 0.5 M H_2SO_4 solution in the presence of 400 ppm CBG-HCl and 800 ppm KI at different exposure time.

Table 5. The IE% and R_P reported from EIS analysis at different exposure times on stainless steel working electrode in the presence of 400 ppm CBG-HCl and 800 ppm KI in a 0.5 M H_2SO_4 solution.

Time (min)	400 ppm CBG-HCl + 800 ppm KI	IE%
	Rp (ohm cm^2)	
30	1079	82.30

60	1569	87.83
120	1590	87.99
240	1625	88.25
360	1633	88.31
1728	1633	88.31

3.5. EDX results and Corrosion inhibition mechanism

The results of EIS and potentiodynamic clearly show that the blend of CBG-HCl-KI inhibitor is an effective stainless steel corrosion inhibitor in a 0.5 M H_2SO_4 solution. Figs. 5 and 6 demonstrate that the CBG-HCl-KI blend acts as an inhibitor of the mixed-type process, eliminating all partial corrosion reactions. The potentiodynamic plots result in Figs 5 and 6. Via the donor-acceptor interaction between the lone pair of electrons on the nitrogen atoms of the CBG-HCl and ions on the stainless steel, inhibitor adsorption occurs. By creating a surface protective layer that minimizes the access of corrosive agents to the surface of SS metal by creating a strong hydrophobic barrier due to the long hydrocarbon (-CH_2) chain, is the mechanism of the inhibition action. The efficiency of inhibition depends on the surface coverage and then the concentration on the metal surface of adsorbed inhibitor molecules. In this respect, EDX measurements were performed on tested SS samples to prove the tightness of the CBG-HCl layer on the SS surface. The EDX findings shown in Fig. 9 and Table 6 show a substantial increase in the carbon and nitrogen percentage (inhibitor atoms content) on the surface of 22 hours SS sample immersed in 0.5 M H_2SO_4 solution at 400 ppm CBG-HCl and 800 ppm KI. This increase in the percentage of components in the stainless-steel sample is proportional to the sum of adsorbed inhibitor molecules on the metal surface.

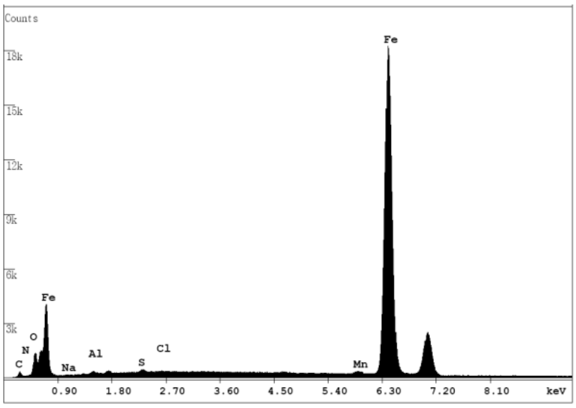

Fig. 9. EDX spectra obtained for stainless steel after 22 hours in 0.5 M H_2SO_4 containing 400 ppm CBG-HCl and 800 ppm KI.

Table 6. Results of EDX spectra display the percentage of weight of carbon and nitrogen atoms on the sample surface obtained for stainless steel after 22 hours in 0.5 M H_2SO_4 containing 400 ppm CBG-HCl and 800 ppm of KI.

Element	wt%	
	Before immersing in inhibited solution	After immersing in inhibited solution
Carbon	0.52	1.55
Nitrogen	0.19	0.91

4. Conclusions

Results from all experiments above led to the next concluded points:

1. Potentiodynamic and EIS experiment results consistently indicated high IE of CBG-HCl-KI blend against the corrosion of the stainless steel in an acidic environment.
2. Potentiodynamic results illustrated that the CBG-HCl-KI blend acts as an inhibitor of the mixed-type process, reducing both cathodic and anodic reactions. The mechanism of inhibition is to shape a surface adsorbed layer as proof of EDX effects, which minimizes the access to the SS surface of solved corrosive agents by the formation of a hydrophobic barrier as a result of the long hydrocarbon chain in CBG-HCl.
3. Measurements of EIS have shown that the inhibitor blend provides a strong long-lasting efficient corrosion inhibition performance at low inhibitor concentrations of continuous immersion of stainless steel in 0.5 M H_2SO_4 solution (400 ppm of CBG-HCl and 800 ppm KI).
4. The inhibitor adsorption mechanism was found to be in very good agreement with the self-assembled monolayer adsorption isotherm of Langmuir adsorption, and the corresponding negative values of standard Gibbs free adsorption energy indicate that the process is spontaneous and involves two forms of interactions, chemisorption and physisorption.
5. This study demonstrated the good inhibition efficiency of CBG-HCl as an environmentally friendly corrosion inhibitor of stainless steel in acidic environment.
6. The simplicity of CBG-HCl synthesis and its stability in an acidic medium also makes its use in industry visible.

Acknowledgements

The corresponding author (A. El Nemr) appreciate the financial support of the current research (Project No. CB-4874 and IG-34795) by the Science and Technological Development Fund (STDF) of Egypt.

References

[1] El Nemr A., New Developments in Electrodeposition and Pitting Research, Research Signpost Publishers, Transworld Research Network, T.C. 37/661(2), Fort P.O., Trivandrum-695 023, Kerala, India (2007). [ISBN 978-81-7895-304-5] 445 pp.

[2] Herle R., Shetty P., Shetty D.S., and Kini A.U., Inhibition of corrosion of stainless steel (304 SS) by *N*-(2-mercaptophenyl)-*N'*-phenyl thiourea in hydrochloric acid. *Indian Journal of Chemical Technology*, **20**(5), 317-322 (2013).

[3] Zhang X., Wang F., He Y., and Du Y., Study of the inhibition mechanism of imidazoline amide on CO_2 corrosion of Armco iron, *Corrosion Science*, **43**, 1417 (2001).

[4] Gusmano G., Labella P., Montesperelli G., Privitera A., and Tassinari S., Study of the inhibition mechanism of imidazolines by electrochemical impedance spectroscopy, *Corrosion*, **62**, 576 (2006).

[5] Sarkar T.K., Saraswat V., Mitra R.K., Obot I.B., Yadav, M., Mitigation of corrosion in petroleum oil well/tubing steel using pyrimidines as efficient corrosion inhibitor: Experimental and theoretical investigation. *Materials Today Communication*, 101862 (2020). https://doi.org/10.1016/j.mtcomm.2020.101862

[6] El Ashry E.S.H., El Nemr A., Essawy S.A., and Ragab S., Corrosion inhibitors Part III: Quantum chemical studies on the efficiencies of some aromatic hydrazides and Schiff bases as corrosion inhibitors of steel in acidic medium, *ARKIVOC, **xi***, 205–220 (2006).

[7] El Ashry E.S.H., El Nemr A., Essawy S.A., and Ragab S., Corrosion inhibitors Part IV: Quantum chemical studies on the corrosion inhibitions of steel in acidic medium by some aniline derivatives, *Chemistry Physics*, **1**, 41–62 (2006).

[8] El Ashry E.S.H., El Nemr A., Essawy S.A., and Ragab S., Corrosion inhibitors Part II: Quantum chemical studies on the corrosion inhibitions of steel in acidic medium by some triazole, oxadiazole and thiadiazole derivatives. *Electrochimica Acta*, **51**(19), 3957-3968 (2006).

[9] El Ashry E.S.H., El Nemr A., Essawy S.A., and Ragab S., Corrosion inhibitors Part V: QSAR of Benzimidazole and 2-substituted derivatives as corrosion inhibitors by using the quantum chemical parameters. *Progress in Organic Coating*, **61**, 11-20 (2008).

[10] El Ashry E.S.H., El Nemr A., and Ragab S., Quantitative structure activity relationships of some pyridine derivatives as corrosion inhibitors of steel in acidic medium, J. Mol. Model., 18 (2012) 1173–1188.

[11] Eddy N.O., Ebenso E.E., El Nemr A., and El Ashry E.S.H., Quantum chemical study of the inhibition of the corrosion of mild steel in H2SO4 by some antibiotics. Journal Molecular Modeling, **15**, 1085–1092 (2009).

[12] El Nemr A., Moneer A.A., Khaled A., El Sikaily A., and Elsayed G.F., Modeling of synergistic halide additives effect on the corrosion of aluminum in basic solution containing dye, *Materials Chemistry and Physics*, 144, 139–154 (2014).

[13] El Nemr A., El Said G.F., Khaled A., El Sikaily A., Moneer A.A., and Abd-El-Khalek D.E., Differences in corrosion inhibition of water extract of Cassia fistula L. pods and *o*-phenanthroline on steel in acidic solutions in the presence and absence of chloride ions. *Desalination and Water Treatment*, **52**(28-30), 5187-5198 (2014). https://doi.org/10.1080/19443994.2013.807473

[14] Sherif E.-S.M., Abbas A.T., Gopi D., and El-Shamy A.M., Corrosion and corrosion inhibition of high strength low alloy steel in 2.0 M sulfuric acid solutions by 3-amino-1,2,3-triazole as a corrosion inhibitor, *Journal of Chemistry*, Article ID 538794, 8 pages (2014) http://dx.doi.org/10.1155/2014/538794

[15] Sherif E.-S.M., Abbas A.T., Halfa H., and El-Shamy A.M., Corrosion of high strength steel in concentrated sulfuric acid pickling solutions and its inhibition by 3-amino-5-mercapto-1,2,3-triazole, *International Journal of Electrochemical Science*, 10, 1777 -1791 (2015).

[16] Elhebshi A., El-Deab M.S., El Nemr A., and Ashour I., Corrosion Inhibition Efficiency of Cysteine-Metal ions Blends on Low Carbon Steel in Chloride-Containing Acidic Media. *International Journal of Electrochemical Science*, **14**, 3897–3915 (2019). https://doi.org/10.20964/2019.03.51

[17] Elhebshi A., El Nemr A., El-Deab M.S., and I. Ashour (2019). CBG-HCl as a green corrosion inhibitor for low carbon steel in 0.5M H_2SO_4 with and without 0.1M NaCl. *Desalination and Water Treatment*, **164**, 240–248 (2019). https://doi.org/10.5004/dwt.2019.24446

[18] Chaubey N., Savita, Qurashi A., Chauhan D.S., and Quraishi M.A., Frontiers and advances in green and sustainable inhibitors for corrosion applications: A critical review, *Journal of Molecular Liquids*, 114385 (2020). https://doi.org/10.1016/j.molliq.2020.114385

[19] Hu J., Zhu Y., Hang J., Zhang Z., Ma Y., Huang H., Yu Q., and Wei J., The effect of organic core–shell corrosion inhibitors on corrosion performance of the reinforcement in simulated concrete pore solution, *Construction and Building Materials*, (2020) https://doi.org/10.1016/j.conbuildmat.2020.121011

[20] Chauhan D.S., Verma C., and Quraishi M.A., Molecular structural aspects of organic corrosion inhibitors: Experimental and computational insights, *Journal of Molecular Structure*, 129374 (2020). https://doi.org/10.1016/j.molstruc.2020.129374

[21] Alrefaee S.H., Rhee K.Y., Verma C., Quraishi M.A., and Ebenso E.E, Challenges and advantages of using plant extract as inhibitors in modern corrosion inhibition systems: Recent advancements, *Journal of Molecular Liquids*, 114666 (2020). https://doi.org/10.1016/j.molliq.2020.114666

[22] Al-Akhras N., and Mashaqbeh Y., Potential Use of Eucalyptus Leaves as Green Corrosion Inhibitor of Steel Reinforcement, *Journal of Building Engineering*, 101848 (2020). https://doi.org/10.1016/j.jobe.2020.101848

[23] Mishra A., J. Aslam, Verma C., Quraishi M.A., Ebens E.E, Imidazoles as highly effective heterocyclic corrosion inhibitors for metals and alloys in aqueous electrolytes: A review, *Journal of the Taiwan Institute of Chemical Engineers*, **114**, 341-358 (2020). https://doi.org/10.1016/j.jtice.2020.08.034

[24] Obot I.B., Solomon M.M., Onyeachu I.B., Umoren S.A., Meroufel A., Alenazi A., and Sorour A.A., Development of a green corrosion inhibitor for use in acid cleaning of MSF desalination plant. *Desalination*, **495**, 114675 (2020). https://doi.org/10.1016/j.desal.2020.114675

[25] Nikoo S.Z., Shockravi A., Ghartavol H.M., Halimehjani A.Z., Ostadrahimi M., Mirhosseini S.M., Behzadi H., and Ghorbani M., A study of Glycine-based dithiocarbamates as effective corrosion inhibitors for cold rolled carbon steel in HCl solutions, *Surfaces and Interfaces,* **21**, 100751 (2020). https://doi.org/10.1016/j.surfin.2020.100751

[26] Ruilin Tang Y.Z.Y.Z., Synthesis and characterization of chitosan based dye containing quaternary ammonium group, *Carbohydrate Polymers*, **139**, 191–196 (2016), https://doi.org/10.1016/j.carbpol.2015.12.047

[27] Yuxiu An G.J.Y.R., An environmental friendly and biodegradable shale inhibitor based on chitosan quaternary ammonium salt. *Journal of Petroleum Science and Engineering*, **135**, 253–260 (2015). https://doi.org/10.1016/j.petrol.2015.09.005

[28] Emam A.E., El-Shamy A.M., Shehata M.F., and Gaballah S.T., Synthesis and Evaluation of Ethyl (4-(N-(Thiazol-2-Yl) Sulfamoyl) Phenyl)Carbamate (TSPC) as a Corrosion Inhibitor for Mild Steel In 0.1M HCl, *Journal of Advanced Chemistry*, **11**(2), 3441-3451 (2015).

[29] Chena Y., Enhanced water-solubility, antibacterial activity and biocompatibilityupon introducing sulfobetaine and quaternary ammonium to chitosan, *Carbohydrate Polymers*, **143**, 246–253 (2016). https://doi.org/10.1016/j.carbpol.2016.01.073

[30] Feng P., Wan K., Cai G., Synergistic protective effect of carboxymethyl chitosan and cathodic protection of X70 pipeline steel in seawater, *RSC Advanced*, **7**, 3419–3427 (2017). https://doi.org/10.1039/c6ra25310e

[31] Eduok U., Ohaeri E., Szpunar J., Conversion of imidazole to N-(3-aminopropyl) imidazole towards enhanced corrosion protection of steel in combination with carboxymethyl chitosan grafted poly(2-methyl-1-vinylimidazole), *Industrial & Engineering Chemistry Research*, **58**, 7179–7192 (2019). https://doi.org/10.1021/acs.iecr.9b00378

[32] Cui G., Chitosan oligosaccharide derivatives as green corrosion inhibitors for P110 steel in a carbon-dioxide-saturated chloride solution. *Carbohydrate Polymers*, **203**, 386–395 (2019). https://doi.org/10.1016/j.carbpol.2018.09.038

[33] Zhao Q., Guo J., Cui G., Han T., Wu Y., Chitosan derivatives as green corrosion inhibitors for P110 steel in a carbon dioxide environment. *Colloids and Surfaces B: Biointerfaces*, **194**, 111150 (2020).

https://doi.org/10.1016/j.colsurfb.2020.111150
[34] Zohdy K.M., El-Shamy A.M., Kalmouch A., and Gad E.A.M., The corrosion inhibition of (2Z, 2′Z)-4,4′-(1,2-phenylene bis (azanediyl))bis(4-oxobut-2-enoic acid) for carbon steel in acidic media using DFT, *Egyptian Journal of Petroleum*, **28**, 355–359 (2019), https://doi.org/10.1016/j.ejpe.2019.07.001
[35] El Nemr A., Impact, Monitoring and Management of Environmental Pollution. Nova Science Publishers, Inc. Hauppauge New York. [ISBN-10: 1608764877, ISBN-13: 9781608764877]. (2011) 638 pages.
[36] El Nemr A., Environmental Pollution and its relation to Climate Change. Nova Science Publishers, Inc. Hauppauge New York. [ISBN-13: 978-1-61761-794-2] (2012) 694 pages.
[37] Shehata O.S., Korshed L.A., and Attia A., Green Corrosion Inhibitors, Past, Present, and Future. Published: December 20th 2017. https://doi.org/10.5772/intechopen.72753
[38] Hassaan M.A., El Nemr A., Health and Environmental Impacts of Dyes: Mini Review, *American Journal of Environmental Science and Engineering*, 1(3), 64-67 (2017).
[39] Zhao X., Qiao Z.-Z., and He J.-X., Preparation of chitosan biguanidine hydrochloride and application in antimicrobial finish of wool fabric, *Journal Engineering Fibers Fabrication*, **5**, 16–24 (2010).
[40] Salama H.E., Saad G.R., and Sabaa M.W., Synthesis, characterization, and biological activity of cross-linked chitosan biguanidine loaded with silver nanoparticles, *Journal Biomaterials Science Polymers Ed*., **27**, 1880–1898 (2016).
[41] Zohdy K.M., El-Sherif R.M., Ramkumar S., and El-Shamy A.M., Quantum and electrochemical studies of the hydrogen evolution findings in corrosion reactions of mild steel in acidic medium, *Upstream Oil and Gas Technology*, **6**, 100025 (2021). https://doi.org/10.1016/j.upstre.2020.100025
[42] Zohdy K.M., El-Sherif R.M., and El-Shamy A.M., Corrosion and Passivation Behaviors of Tin in Aqueous Solutions of Different pH, *Journal of Bio- and Tribo-Corrosion*, 7:74 (2021). https://doi.org/10.1007/s40735-021-00515-6
[43] Choi D., You S., and Kim J., Development of an environmentally safe corrosion, scale, and microorganism inhibitor for open recirculating cooling systems, *Materials Science and Engineering A*, 335, 228 (2002).
[44] Omanovic S., and Roscoe S.G., Effect of linoleat on electochemical behavior of stainless steel in phosphate buffer, *Corrosion*, **56**, 684 (2000).
[45] Moretti G., Guidi F., and Grion G., Tryptamine as a green iron corrosion inhibitor in 0.5 M deaerated sulphuric acid, *Corrosion Science*, **46**, (2004) 387.
[46] Aramaki K., and Shimura T., Self-assembled monolayers of carboxylate ions on passivated iron for preventing passive film breakdown, *Corrosion Science*, **46**, 313 (2004).
[47] El Nemr A., El-Sikaily A., and Khaled A., Modeling of adsorption isotherms of Methylene Blue onto rice husk activated carbon. *Egyptian Journal of Aquatic Research*, **36**(3), 403-425 (2010).
[48] Ghareba S., and Omanovic S., Interaction of 12-aminododecanoic acid with a carbon steel surface towards the development of ‘green’ corrosion inhibitors, *Corrosion Science*, **52**, 2104–2113 (2010).
[49] Mahapatro A., Johnson D.M., Patel D.N., Feldman M.D., Ayon A.A., Agrawal C.M., Surface modification of functional self-assembled monolayers on 316L stainless steel via lipase catalysis, *Langmuir*, **22**, 901 (2006).
[50] Raman A., Dubey M., Gouzman I., and Gawalt E.S., Formation of self-assembled monolayers of alkylphosphonic acid on the native oxide surface of SS316L, *Langmuir*, **22**, 6469 (2006).
[51] Raman A., and Gawalt E.S., Self-assembled monolayers of alkanoic acids on the native oxide surface of SS316L by solution deposition, *Langmuir*, 23, 2284 (2007).